Design and Testing of a Permanent Magnet
Axial Flux Wind Power Generator

Garrison F. Price, Todd D. Batzel, Mihai Comanescu, and Bruce A. Muller
Pennsylvania State University, Altoona College
gfp5001@psu.edu , tdb120@psu.edu, muc23@psu.edu, bam4@psu.edu

Abstract

The axial flux (disc shape) permanent magnet machine is an attractive alternative to radial flux (cylindrical shape) machines in wind turbine applications. The axial flux configuration is amenable to the low-speed, high-torque operation of a direct drive wind energy system. Direct drive wind energy conversion tends to decrease the system size, weight, and noise, while increasing overall efficiency and reliability.

When computing the magnetic field in axial field electric machines for machine design purposes, a 3-D electromagnetic finite element analysis (FEA) is generally required. However, FEA typically requires very long computation time, especially for 3-D computations. Furthermore, developing a proficiency in the use of electromagnetic FEA tools is not realistic for most undergraduate engineering technology students in a single semester. Therefore, an analytical model of the axial field machine that facilitates expeditious machine design and modeling is highly desirable. In this paper, the magnetic field distribution in a two-rotor, permanent magnet, ironless stator axial field generator for direct-drive wind energy conversion is studied. The goal is to develop the analytical model for the machine that will facilitate timely design trade-off studies and support an overall electro-mechanical model of wind energy conversion systems.

With the analytic solution for magnetic field strength in the airgap, other quantities of interest may be evaluated, such as back emf (voltage due to rotor magnetic field plus mutual and self-induced voltage between windings), its harmonic content, and, consequently, the machine torque. With this approach, it is possible to analyze the entire electro-mechanical system, simulating rotation, quickly calculating magnetic fields, torques, and voltages for specified electrical loading conditions.

Based on the analytical design approach, an experimental micro-wind generator is constructed. The predicted performance metrics from the analytical model are then compared with experimentally measured quantities to evaluate the effectiveness of the analytical approach.

1. Introduction

Design of permanent magnet machines, such as the permanent magnet axial flux generator, is a procedure involving iterative computations based on performance requirements and trade-

offs. Typically, empirical relations or simplified models are used in the early stages of the design, followed by finite element analysis (FEA) in the later stages. In either case, calculation of the airgap magnetic field is of utmost importance because it is required for the calculation of performance metrics, such as torque constant, torque ripple, back emf constant, and back emf waveshape.

Calculation of the airgap magnetic field using FEA is quite time consuming, especially for an axial flux permanent magnet machine, since 3-D FEA is generally required. As a result, analytical methods to obtain magnetic field solutions have been presented in the literature for permanent magnet synchronous machines of radial flux [1, 2], linear [3, 4], and axial flux configuration [5, 6, 7]. However, solutions proposed for axial flux machines [8, 9, 10] use a mean radius approach, which limits the accuracy of the solution for machines whose relative magnet width or stator coil width is a function of stator radius.

In this paper, the magnetic field distribution in a two-rotor, permanent magnet, ironless stator axial field generator for direct-drive wind energy conversion is studied. The goal is to develop the analytical model for the machine that will facilitate timely design trade-off studies and support an overall electro-mechanical model of energy conversion system. The model will also consider machine designs where magnet and coil width relative to the pole pitch varies with the machine radius. Analytical results will be validated through a combination of finite element analysis (FEA) and a series of experiments to demonstrate the usefulness of the proposed method.

2. Permanent Magnet Axial Flux Machines

Axial flux machines are formed by a rotor disc carrying magnets that produce an axial flux and a stator disc containing the phase windings. Many variations in this basic design are possible, including single-sided [11], double-sided [12], torus [13, 14], and multi-disc designs [15]. This paper focuses on the two-rotor, one stator topology, where a single stator is placed between two permanent magnet (PM) rotor discs, as shown in Figure 1. This figure shows a view looking inward radially. Figure 2 shows rotor and stator views looking in the axial direction.

The two disc shaped rotors of Figure 1 carry axially magnetized, surface mounted NDFeB magnets on their inner surfaces. The magnets on opposing rotor discs are arranged so that a North pole on one rotor faces a South pole on the other, resulting in an axial magnetic field so that stator yoke is not required (stator is required for N-N facing magnets). In the absence of stator iron, three-phase coils are typically potted in a resin. This construction has several advantages over other topologies, such as ease of manufacture, reduced iron losses, and no cogging torque. The double-rotor, single stator axial flux machine also has relatively high moment of inertia, allowing energy to be stored in the rotating machine to help smooth power output during transients.

3. Analytical Model of Axial PM Machine

To analyze the magnetic field in the airgap of the axial PM machine, computations based on the work in reference [6] are applied. However, the analytic model presented in reference [6]
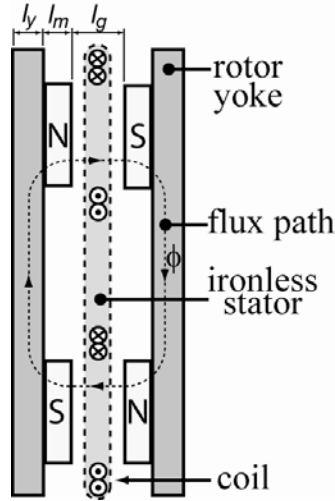
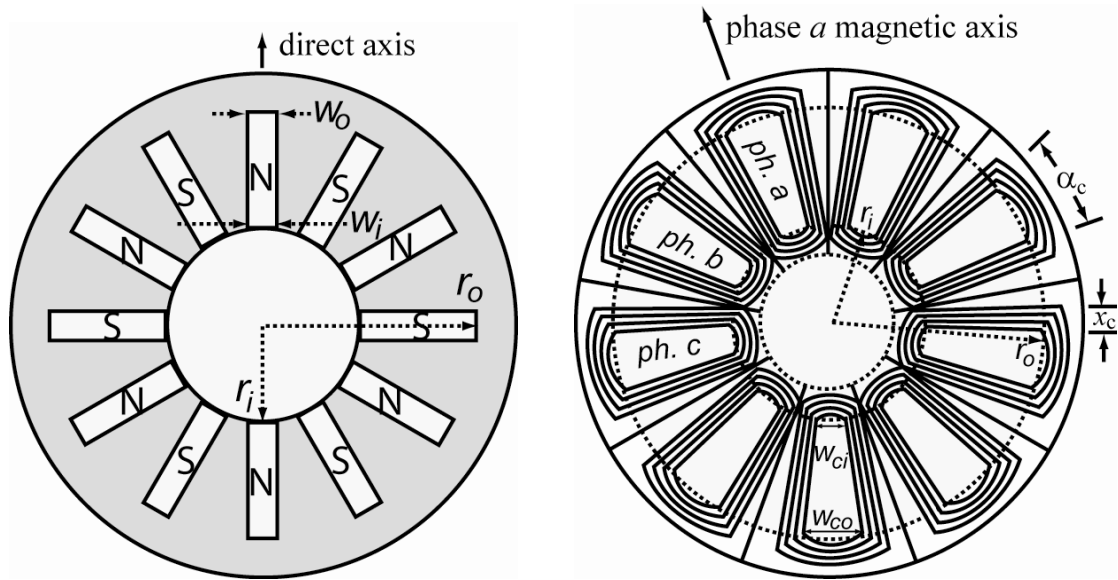Figure 1. Construction of dual-rotor axial PM generator (looking inward radially)

Figure 2. Construction of dual-rotor axial PM generator: rotor (left) and stator (right)

assumes the presence of stator iron and that the field intensity in circumferential direction is zero at all iron boundaries (stator and rotor). In the case of the ironless stator studied in this paper, the only two iron boundaries are the rotor yokes. Thus, the equations developed in [6] are modified by applying superposition; that is, the field is determined by summing the fields resulting from the magnets of each rotor side acting individually and the armature reaction field. Although superposition does not apply if saturation occurs, ironless armature machines would not normally be operating in the saturation condition due to the relatively large airgap in such machines.

While previous analytical studies of the axial PM machine have typically used the mean radius to analyze the axial gap machine in 2-D, a more precise method of dividing the machine into radial slices (quasi-3-D) is applied here. Using this approach, the magnetic field

is calculated over a range of radii (or slices), assuming no radial component of magnetic field. This assumption is reasonable for a non-saturated operation because an ironless stator machine is not normally operating in a saturated condition. The quasi-3-D approach is expected to improve accuracy as compared with the mean radius approach—especially in cases where the relative magnet width varies with the machine radius.

3.1 Magnetic Field Due to Permanent Magnets

In this section, an analytic expression for airgap magnetic flux density is determined using the coordinate system shown in Figure 3, which is a cross-sectional view of the machine looking inward radially. The x and y coordinates in Figure 3 represent the circumferential and axial directions, respectively. Following the analytical method presented in reference [6], with appropriate modifications as described previously, the space harmonic (indicated by subscript n) flux densities at position y due to the magnets on rotors 1 and 2 are found to be, respectively,

$$B_{yn1}(x) = \left(\frac{\hat{J}_n \mu_0 \sinh(u_n l_m)}{u_n \sinh(u_n Y_2)} \cosh(u_n(Y_2 - y)) \right) \cos(u_n x) \tag{1}$$

$$B_{yn2}(x) = \left(\frac{\hat{J}_n \mu_0 \sinh(u_n l_m)}{u_n \sinh(u_n Y_2)} \cosh(u_n(y)) \right) \cos(u_n x) \tag{2}$$

where

$$Y_2 = l_g + 2l_m \tag{3}$$

$$u_n = 2\pi n / \lambda \; ; \lambda = 2\pi R_m / p \; . \tag{4}$$

Also, p represents the number of pole pairs, R_m is mean core radius for the radial slice under consideration, and $\hat{J}_n$ is the equivalent current sheet due to magnets 1 or 2. The total flux density for each slice of the machine is determined by the superposition of equation (1) and equation (2). The magnets for each radial slice are modeled as an equivalent current sheet:

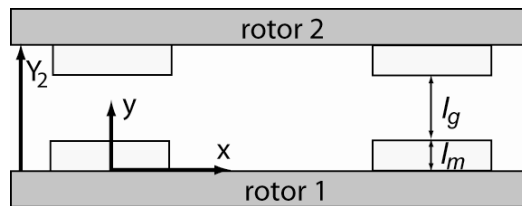$$\hat{J}_n = \frac{4B_r}{\tau_p \mu_0 \mu_{rec}} \sin\left(\frac{n\pi\tau_m}{2\tau_p} \right) \tag{5}$$

Figure 3. Model and coordinate system for magnetic flux density distribution

where τ_m and τ_p are the magnet and pole pitches, respectively, for the radial slice under consideration. The terms B_r and μ_{rec} are the remanant flux density and permeability, respectively, of the permanent magnet. The total flux densities due to magnets on rotors 1 and 2 for a single radial slice are the sum of space harmonics:

$$B_{y1}(x) = \sum_{n=1} B_{yn1}(x) \; ; \; B_{y2}(x) = \sum_{n=1} B_{yn2}(x) \,. \tag{6}$$

3.2 Magnetic Field Due to Armature Reaction

The analytic expression for magnetic field due to armature reaction, not including contributions due to the rotor permanent magnets, will be developed in this section. The model and coordinate system used to develop the analytic expressions is shown in the cross-sectional view of Figure 4. The approach developed in reference [6] is once again applied with modification for the armature reaction analysis. In this case, the armature conductors are represented by a current sheet K, whereas in the previous section, it was the permanent magnets that were modeled as a current density J. Armature coils are represented by a current sheet with a peak value $\hat{K}$ located at the mean axial position $y_c = \dfrac{Y_2}{2}$. The flux density at the mean axial position using Fourier analysis is

$$B_{n-arm}(x) = \hat{K}_n \mu_0 \left(\frac{\cosh(u_n Y_c)}{\sinh(u_n Y_2)} \cosh(u_n (Y_2 - y)) \right) \cos(u_n x) \,, \tag{7}$$

where the linear current density function is

$$K(x) = \sum \hat{K}_n \sin(u_n x). \tag{8}$$

The peak current density is

$$\hat{K}_n = \frac{Ni}{x_c} \frac{4}{n\pi} \sin\left(\frac{n\alpha_c}{2} \right) \sin\left(\frac{nx_c p}{4R_m} \right), \tag{9}$$
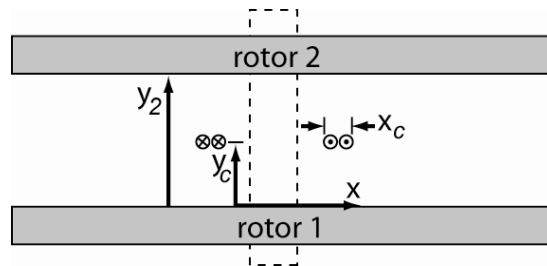

Figure 4. Model and coordinate system for armature (looking inward radially)

where N is the number of turns per coil, i is the current in each individual conductor in the coil; x_c is the coil conductor bundle width in the circumferential direction; and α_c is the average coil span in electrical radians. The Fourier coefficients corresponding to the current sheet density can be plugged directly into equation (7) to calculate the flux density due to the armature conductors.

Note that the coil span may vary with radius for certain types of coil design. For this reason, the armature reaction is evaluated for several radial slices, as described previously, to determine the armature reaction field at various radii. The total flux density due to armature reaction for a single slice is the sum of the space harmonic components:

$$B_{arm}(x) = \sum_{n=1} B_{n-arm}(x) \tag{10}$$

Finally, the net airgap flux density per radial slice can be calculated using superposition by adding the contributions of both magnet sides (equations 1 and 2) with the armature reaction contribution (equation 10).

3.3. Computation of Generator Parameters

Once the net field solution is obtained (due to rotor field and armature reaction), other quantities of interest may be evaluated, such as back emf, the machine torque, and torque ripple. With this approach, it is possible to analyze the entire electro-mechanical system for any specified operating condition and simulating rotation, as well as to quickly calculate magnetic fields, torques, armature currents, and voltages.

To determine the back emf, the flux linking each coil can be determined from the solution for net airgap flux density. The magnetic flux linking a coil in a single radial slice of the machine is a function of the rotor angle θ and can be expressed as

$$\lambda_{slice}(\theta) = N \iint_S B \cdot dS \ , \tag{11}$$

where S is the surface inside the coil for the radial slice under consideration. Numerically, this is calculated using the cross-sectional area enclosed by the coil slice. The total flux linking the entire coil is then determined by summing the flux linking each radial slice,

$$\lambda_{coil}(\theta) = \sum_1^{slices} \lambda_{slice}(\theta) \ . \tag{12}$$

By carrying out the magnetic field calculations in a time-stepping fashion with a changing rotor angle θ, the flux linking each coil can be determined at each time step. The induced emf in the coil is determined directly by Faraday's Law:

$$e_{coil}(t) = \frac{\Delta \lambda_{coil}}{\Delta t} \ . \tag{13}$$

Since a phase winding is comprised of a combination of series or parallel coils whose induced voltages are in phase with one another, the total per phase induced emf e_{phase} is determined by multiplying the coil emf by the total number of series coils per phase:

$$e_{phase}(t) = \sum_{1}^{\text{series coils}} e_{coil}(t) \qquad (14)$$

The computation of the electromechanical torque developed by the generator may then be determined by using the instantaneous phase voltages and armature currents, where armature currents depend on the electrical loading of the generator:

$$T(t) = \frac{1}{\omega_m} \sum_{1}^{m} e_{phase}(t) i_{phase}(t) . \qquad (15)$$

Here, m is the number of generator phases, and ω_m is the shaft speed (rad./s).

4. Axial PM Machine Design and Analysis

In this section, the analytical approach described in section 3 is applied to a representative axial flux wind generator that was constructed and tested in a laboratory setting. The experimental results are compared with those obtained analytically to evaluate the effectiveness of the proposed analytical model. The results may be used to optimize the generator design for its intended application.

The rotor and stator are constructed as shown in Figure 2, with magnet and coil dimensions given in Table 1. This initial design was chosen because it contains readily available, low-cost components. The dimensions were obtained from a commercially available small-scale wind turbine rated at 750 W for a turbine speed of 600 RPM. This generator design is suited for charging a 12-volt battery system with the rectified generator output voltage at speeds down to 140 RPM. There are nine identical coils with 36 series turns, each with rated current

Table 1. Dimensions of experimental PM generator

Dimension	Value
l_m	.0127 m
l_g	.01905 m
l_y	.00635 m
r_o	.1524 m
r_i	.1016 m
w_o	.0254 m
w_i	.0254 m
w_{ci}	.02032 m
w_{co}	.0254 m

capacity of approximately 10 A rms. Three series coils per phase are arranged, as indicated in Figure 2, and the phases are connected in the Y configuration. The windings are short-pitch, concentrated coils, which are widely used due to ease of construction. As indicated in Figure 2, three armature coils occupy the same circumferential area as four permanent magnet poles. Note also that the airgap length (l_g) is approximately equal to the effective magnet height ($2l_m$) so that the permanent magnet operating point is near the maximum power product [10].

4.1 Magnetic Field in Generator at No Load

The analytic magnetic field computations described in equations (1) and (2) are now used to determine the no-load airgap flux density in the experimental machine. As a base-line, these analytic results are compared to magnetic FEA solutions.

Figure 5 shows the flux density determined by the analytical method compared with FEA results for both the innermost slice (smallest radius) and outermost slice (largest radius). From the figure, it is clear that the analytic result closely matches the FEA computation. It should also be noted that the flux density at the outer slice has a more pronounced peak than the inner radius, since the relative magnet width per pole pitch varies with radius. This feature is not captured using the mean radius approach of other analytic solutions.

In Figure 6, analytically calculated flux density over a magnetic pole pair is mapped versus the axial machine radius. This mapping was generated by calculating the field at 10 discrete radial slices and using those results to form the 2-D result shown in the figure. The figure illustrates the importance of the magnet shape because the peaks shown in the map closely resemble the rectangular magnet dimensions.

The variation of airgap flux density in a single slice versus axial distance from the permanent magnet surface is shown in Figure 7. The first plot compares flux densities at the magnet surface and at the airgap midpoint. The second plot shows a mapping of flux density over a
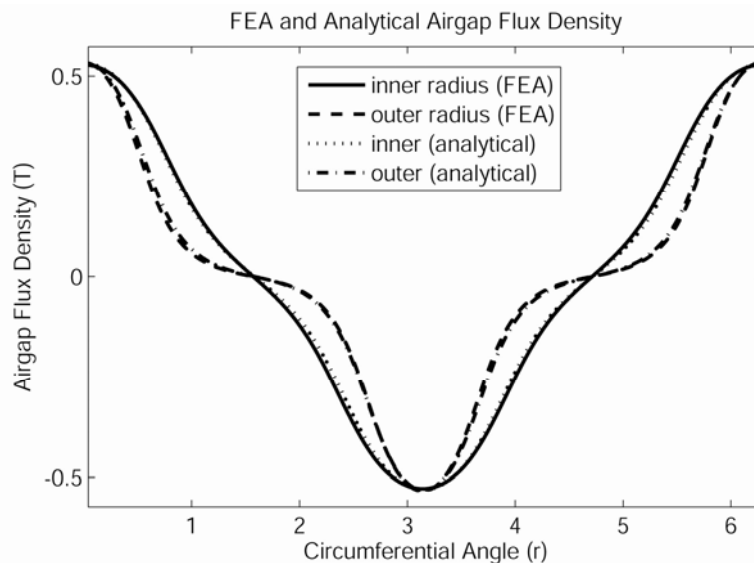

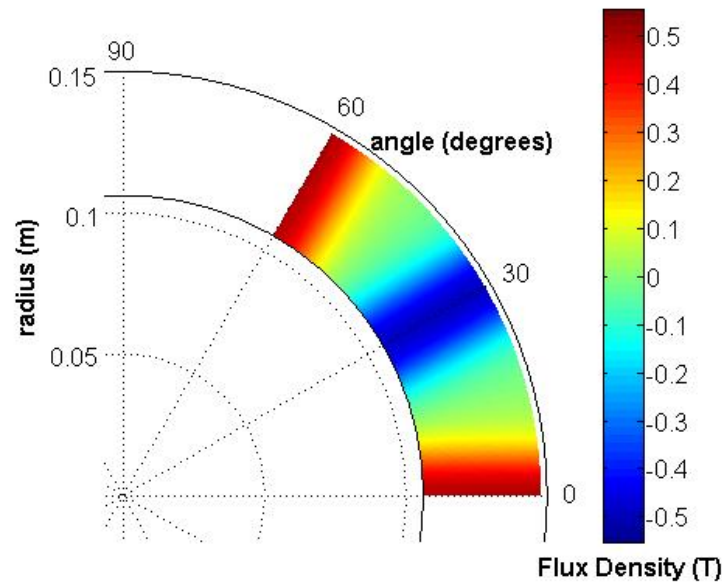Figure 5. Flux density comparison with FEA results for several radial slices

Figure 6. Airgap flux density (normal component) over one pole pair versus radius

pole pair versus the axial distance from the magnet surface. This mapping demonstrates how the flux spreads out near the center of the airgap.

4.2 Magnetic Field in Generator Under Load

In this section, the analytic armature reaction magnetic field computation of equation (7) is applied to the experimental machine. To demonstrate the results, analysis is performed at rated maximum current of 10 A rms in the phase *a* winding and –5 A in the other two phases to satisfy the zero sequence current requirement of a Y-connected armature. The corresponding current sheet for this armature operating condition is shown in Figure 8.

After calculating the Fourier coefficients corresponding to the current sheet, equation (7) is used to find the airgap flux density due to the armature currents. The armature reaction field under the phase *a* coil for rated current is shown in Figure 9. The figure shows peaks near the edge of the phase band and an average value of .004 Tesla. Comparing Figure 9 with Figure 5, it is clear that the armature reaction field is significantly smaller than the field produced by the permanent magnets. This is a characteristic of the slotless, ironless core machine and was confirmed in [16]. Since the average magnitude of the armature reaction is insignificant compared to the permanent magnet field, it is reasonable to neglect armature reaction to simplify remaining calculations of machine performance.
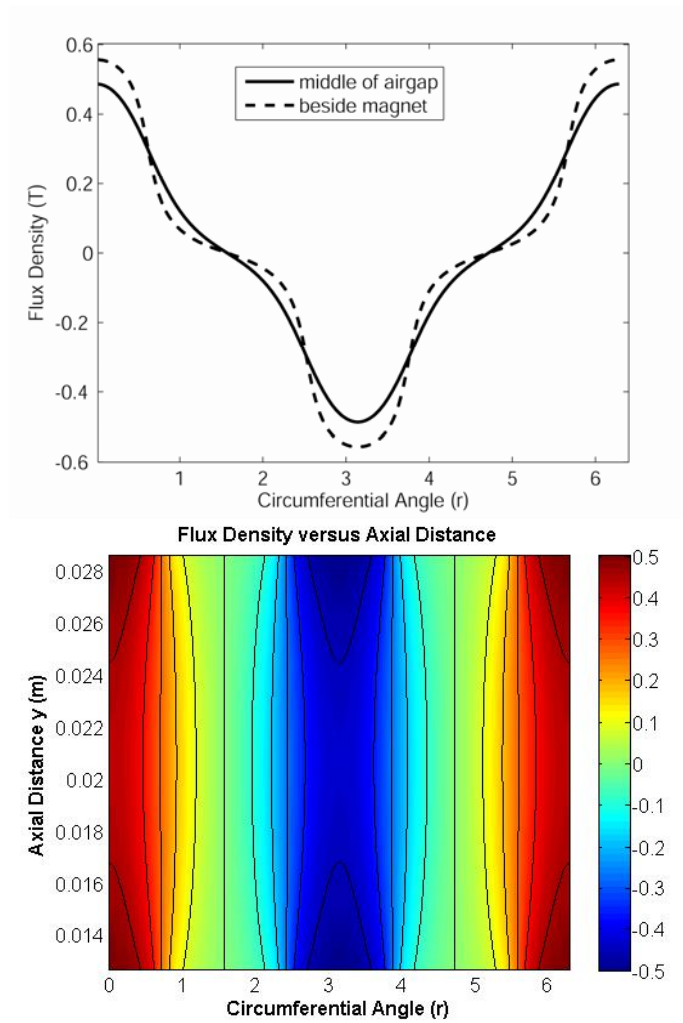
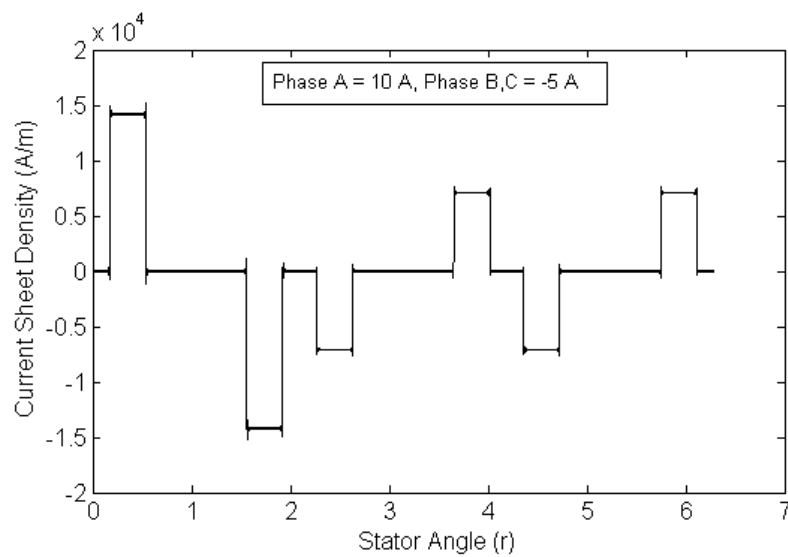Figure 7. Airgap flux density (normal component) versus axial position (*y*)

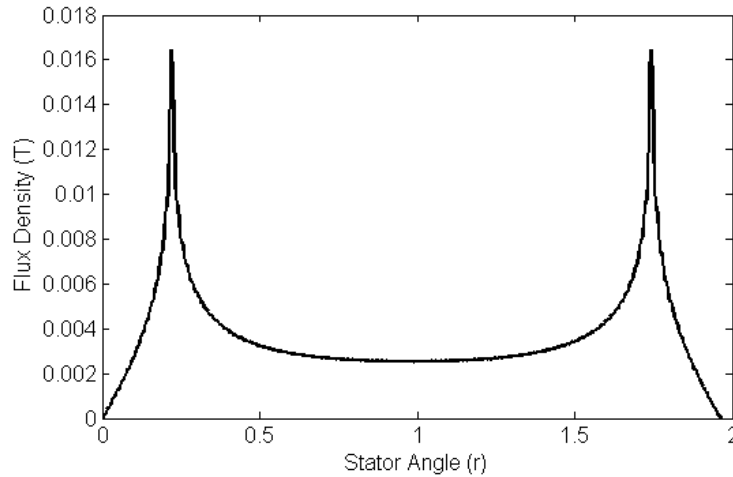Figure 8. Current sheet density over a stator magnetic cycle

Figure 9. Armature reaction field distribution for rated current in a single phase

4.3 Induced Phase Voltage

Given the analytical solutions for airgap flux density, the induced back emf per phase may now be predicted using equation (14). Using the time-stepping approach described previously and a rotational speed of 600 RPM, the airgap fields were calculated for each rotational position. The resulting back emf prediction is shown in Figure 10. In this figure, the trapezoidal coil, whose dimensions are included in Table 1, are compared with a rectangular coil to demonstrate the importance of the coil shape in the generator design.

5. Experimental Results

The analytically predicted values of the generator performance are now verified experimentally. Although the magnetic field solutions cannot easily be verified experimentally, they have been favorably compared with a magnetic FEA solution. Similarly,
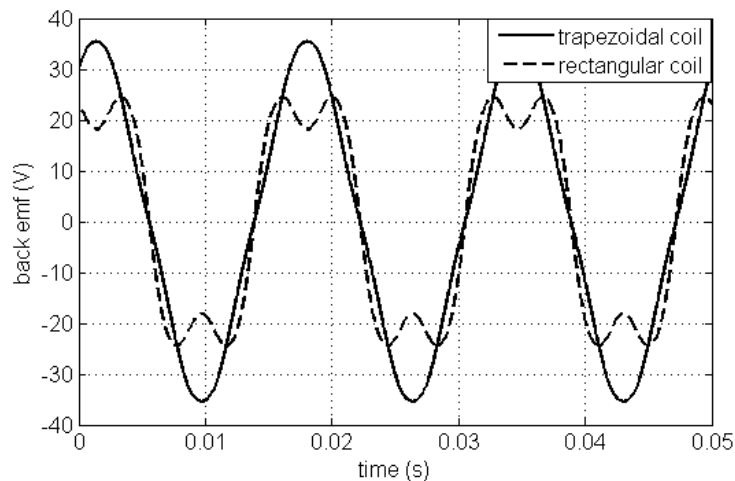

Figure 10. Predicted back emf at 600 RPM for two coil shapes

torque ripple is not easily measurable. Therefore, the focus here is on comparison of predicted back emf and torque (amplitude and wave shape) with the directly measured values.

To experimentally measure the back emf, the setup shown in Figure 11 is used. The apparatus includes the constructed axial flux generator (at the left) coupled with a prime mover through a belt arrangement. The prime mover is a variable speed DC motor, which is at the far right in the figure. The steady state shaft torque is obtained by the product of prime mover current and torque constant.

With the prime mover rotating the generator shaft at 600 RPM, the no-load per-phase back emf, shown in Figure 12, was obtained. The waveform is sinusoidal with a peak value of 37 volts. This compares favorably with the predicted back emf value of 35.5 volts for the trapezoidal coil (which is used in the laboratory experiment) shown in Figure 10. Although not shown here, a second generator that uses a more rectangular coil design was shown experimentally to generate a back emf waveform that closely resembles the predicted voltage

Figure 11. Laboratory setup for wind generator experiments
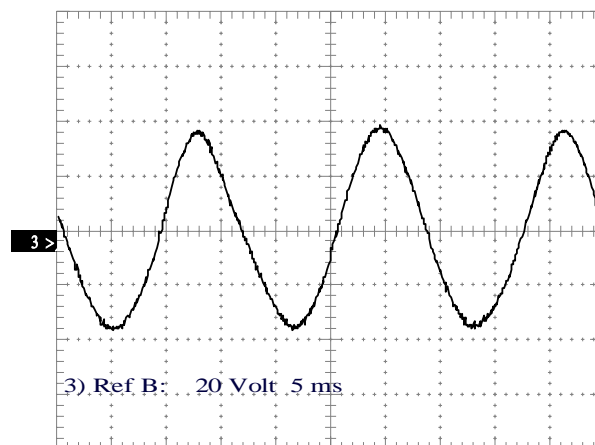

3) Ref B: 20 Volt 5 ms

Figure 12. Measured single-phase back emf at 600 RPM, no load

shown in Figure 10 for the rectangular coil. This convincing comparison helps to confirm the value of the analytical method.

To verify the analytical prediction that armature reaction effects are negligible, the generator was loaded electrically to rated current at unity power factor and a speed of 500 RPM. Figure 13 shows the comparison between the no-load back emf at 500 RPM and the rated load emf at the same speed. The figure shows no noticeable difference between the voltage waveforms at no-load and rated load (for purpose of display, the dc offset was added to the oscilloscope so that the two waveforms were separated).

The measured average shaft torque at 500 RPM and rated load current was 12.6 n-m, which compares favorably with the analytically predicted torque of 12.8 n-m, shown in Figure 14, for the trapezoidal coil design. Note that the predicted torque ripple is rather low (1.1 percent) for the trapezoidal coil design carrying sinusoidal current as used in the laboratory experiments. The torque predictions for the rectangular coil in Figure 14 assume rectangular phase current and yield higher-than-average torque at the expense of increased torque ripple. The actual torque ripple could not be experimentally ascertained.
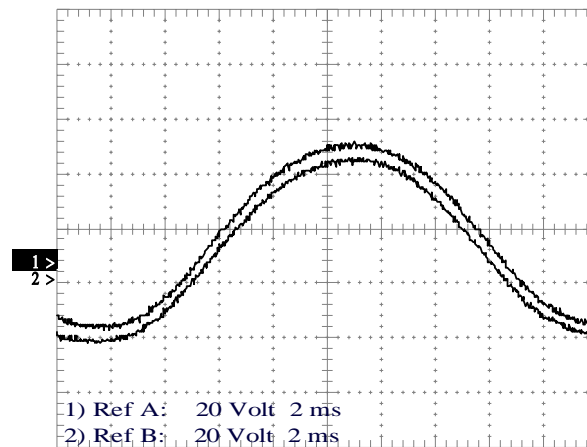

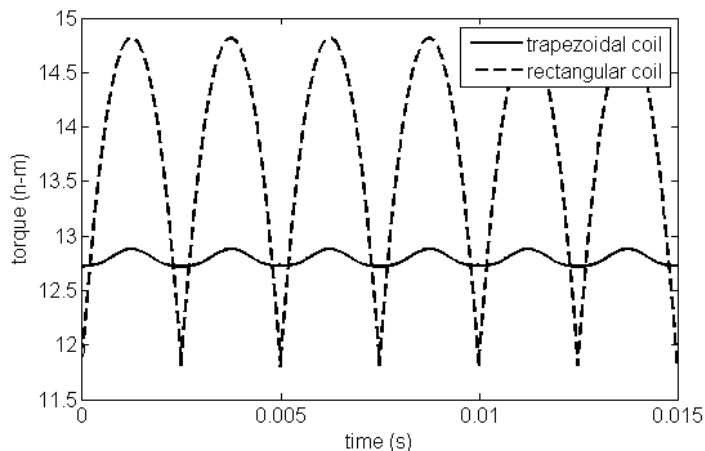Figure 13. Comparison of no-load and full-load back emf at 500 RPM

Figure 14. Predicted instantaneous torque at 500 RPM full load for two coil shapes

6. Conclusion

An analytical approach for the calculation of airgap magnetic fields in an ironless stator axial flux permanent magnet machine has been developed. The proposed analysis is carried out using radial slices, rather than a mean radius approach, so that increased accuracy is possible for machines whose relative magnet or coil width varies with radius. From the magnetic field solutions, which are validated by comparison with FEA results, techniques for predicting generator performance features such as torque, torque ripple, and back emf waveshape have been developed. The accuracy of the proposed approach is analyzed by comparing analytical predictions with experimentally measured results on an axial flux permanent magnet generator. The predicted emf amplitude and waveshape agrees with the emf measured on the actual generator for several coil shapes. The analytically predicted steady state torque is also consistent with the experimental measurements. The close correlation of predicted generator performance and experimental results suggests that the proposed analytical method is a viable alternative to time-consuming FEA analysis for the early stages of ironless stator PM axial flux machine design.

7. References

[1]   Proca, A.B., A. Keyhani, A. El-Antably, W. Lu, and M. Dai, "Analytical model for permanent magnet motors with surface mounted magnets," *IEEE Transactions On Energy Conversion*, vol. 18, no. 3, Sept. 2003, pp. 386–391.

[2]   Rosu, M, A. Arkkio, T. Jokinen, J. Mantere, and J. Westerlund, "Prediction of airgap magnetic field distribution in large output power permanent magnet synchronous motor," *Electromotion '99 - 3rd International Symposium on Advanced Electromechanical Motion Systems*, vol. 1, July 1999, pp. 179–184.

[3]   Jung, S., J. Chun, and H. Jung, "Performance evaluation of slotless permanent magnet linear synchronous motor energized by partially excited primary current," *IEEE Trans. On Magnetics*, vol. 37, no. 5, Sept. 2001, pp. 3757–3761.

[4]   Virtic, P, and B. Stumberger, "Analytical analysis of magnetic field and force calculation in a slotless-type permanent magnet linear synchronous machine; verification with numerical analysis," *IEEE International Electric Machines & Drives Conference*, vol. 2, May 2007, pp. 963–968.

[5]   Furlani, H.P., "Computing the field in permanent-magnet axial-field motors," *IEEE Transactions on Magnetics*, vol. 30, no. 5, Sept 1994, pp. 3660–3663.

[6]   Bumby, J.R., R. Martin, M.A. Mueller, E. Spooner, N.L. Brown, and B.J. Chalmers, "Electromagnetic design of axial-flux permanent magnet machines," *IEEE Proc. on Power Applications*, vol. 151, n. 2, pp. 151–160, March 2004.

[7]   Chan, T.F., and L.L. Lai, "An axial-flux permanent-magnet synchronous generator for a direct-coupled wind-turbine system," *IEEE Trans. on Energy Conversion*, vol. 22, no. 1, March 2007, pp. 86–94.

[8]   Zhang, Y.J, S.L. Ho, H.C. Wong, and G.D. Xie, "Analytical prediction of armature-reaction field in disc-type permanent magnet generators," *IEEE Trans. on Energy Conversion*, vol. 14, no. 4, Dec. 1999, pp. 1385–1390.

[9] Chan, T., S. Xie, and L.L. Lai, "Computation of no-load and armature reaction fields of an axial-flux permanent-magnet synchronous generator," *IEEE International Electric Machines & Drives Conference*, vol. 1, July 2007, pp. 1–6.

[10] Gieras, J.F., R. Wang, and M.J. Kamper, "Axial flux permanent magnet brushless machines," Kluwer Academic Publishers, 2004.

[11] Patterson, D., and R. Spee, "The design and development of an axial flux permanent magnet brushless DC motor for a wheel drive in a solar powered vehicle," *Proc. IEEE Ind. Apps. Society Conf.*, Denver, 1994, vol. 1, pp. 188–195.

[12] Brown, N., L. Haydock, and J.R. Bumby, "Foresight vehicle: A toroidal, axial flux generator for hybrid IC engine/battery electric vehicle applications." Proc. SAE Conf. paper 2002-01-089, Detroit, March 2002.

[13] Spooner, E. and B.J. Chalmers, "TORUS: A slotless, toroidal-stator permanent magnet generator," *IEE Proc. Electr. Power Appl.*, Nov. 1992, pp. 497–506.

[14] Huang, S., M. Aydin, and T.A. Lipo, "TORUS concept machines: pre-prototyping design assessment for two major topologies," *2001 IEEE Industry Applications Conference*, vol. 3, no. 30, Sept. 2001, pp. 1619–125.

[15] Kessinger, R., and S. Robinson, "SEMA-based permanent magnet electric motors for high torque, high performance," *Naval Symposium on Electric Machines*, Newport, RI, 1997, pp. 151–155.

[16] Azzouzi, J., Barakat, G., and B. Dayko, "Quasi-3D analytical modeling of the magnetic field of an axial flux permanent-magnet synchronous machine, *IEEE Trans. On Energy Conversion*, vol. 20, no. 4, Dec. 2005, pp. 746–752.

GARRISON F. PRICE is currently a fourth-year student in the Electro-Mechanical Engineering Technology program at Penn State Altoona. His primary research interest is in wind energy systems and applications.

TODD D. BATZEL received a BS in Electrical Engineering from the Pennsylvania State University in 1984, an MS in Electrical Engineering from the University of Pittsburgh in 1989, and a PhD in Electrical Engineering in 2000 from the Pennsylvania State University. He is currently an Associate Professor of Electrical Engineering at Penn State Altoona. His research interests include machine controls, electric drives, artificial intelligence, and distributed computing.

MIHAI COMANESCU received his BSEE from Bucharest Polytechnic University in 1992 and his MS and PhD from the Ohio State University in 2001 and 2005, respectively. He is currently an Assistant Professor of Electrical Engineering at Penn State Altoona. His research interests are in power electronics, ac drives, and motion control systems.

BRUCE A. MULLER received his BSME from Rutgers University in 1978 and his M. Eng. in Industrial Engineering in 1986 from the Pennsylvania State University. He is currently a senior instructor in Engineering at Penn State Altoona. His primary research interest is the application of alternative energy technologies.